Desalination and Water Treatment
www.deswater.com

doi:10.5004/dwt.2017.20299

69 (2017) 190–201
March

Theoretical and experimental study of multi-effect vacuum membrane distillation systems for liquid desiccant air conditioning and zero liquid discharge

Florian Kiefer[a,*], Florian Schummer[b], Alexander Präbst[a], Markus Spinnler[a], Thomas Sattelmayer[a]

[a]*Lehrstuhl für Thermodynamik, Technische Universität München, Boltzmannstr. 15, 85748 Garching, Germany, Tel. +498928916252, email: kiefer@td.mw.tum.de (F. Kiefer), praebst@td.mw.tum.de (A. Präbst), spinnler@td.mw.tum.de (M. Spinnler), sattelmayer@td.mw.tum.de (T. Sattelmayer)*

[b]*Technische Universität München, Boltzmannstr. 15, 85748 Garching, Germany, email: florian.schummer@live.de (F. Schummer)*

Received 12 July 2016; Accepted 24 October 2016

ABSTRACT

Since its first description in literature, a variety of different system configurations for distillation over hydrophobic membranes have been invented. General advantages are the applicability at relatively low operation temperatures, low fouling potential, high product quality and the possibility to operate the system at very high feed concentration. This is why membrane distillation (MD) is applied more and more in the field of zero liquid discharge. One main drawback of MD, the low specific distillate production, can be partially overcome by using a vacuum enhanced process. Furthermore, with help of a multi-effect arrangement as known from multi-effect distillation (MED) or multi-stage flash (MSF), energy efficiency can be significantly enhanced. For application in seawater desalination, the vapor pressure reduction of the treated feed waters is mainly limited by the solubility limit of sodium chloride. For electrolyte solutions used for air dehumidification in liquid desiccant air conditioning (LDAC), much lower vapor pressures are reached, which significantly reduces the performance of thermal regeneration systems. With the aim of efficiency enhancement of desiccant regeneration in LDAC an experimental study has been conducted on a vacuum multi-effect membrane distillation system. As desiccant an aqueous solution of calcium chloride up to 45 m% has been used. A systematic sensitivity analysis on feed concentration, temperature levels and number of effects shows the operation limits of the plant. Especially for high feed concentrations, the number of stages shows a significant influence on the process performance.

Keywords: Vacuum membrane distillation; Multi-effect; Zero liquid discharge; Liquid desiccant air conditioning; Experiment

1. Introduction

The treatment of concentrated aqueous electrolyte solutions such as reverse osmosis (RO) brines or other saline waste waters has become of high interest during the last years. Beyond the operating limit of RO, membrane distillation (MD), as a low temperature thermal desalination technique, has shown promising results. Therefore, many publications on zero liquid discharge (ZLD) with MD can be found. The capability to treat salt solutions up to their solubility limit is one of the main strengths of this technique. The significant vapor pressure reduction at elevated concentrations affect the performance of the desalination

---

*Corresponding author.

Presented at the EDS conference on Desalination for the Environment: Clean Water and Energy, Rome, Italy, 22–26 May 2016.

system and creates the necessity to focus on better energy recovery to enhance efficiency of the process.

Despite that, the reduction of the equilibrium vapor pressure over salt solutions such as aqueous lithium or calcium chloride is used in air conditioning applications. So called liquid desiccant air conditioning (LDAC) uses aqueous solutions of about 40 m% LiCl or $CaCl_2$ for air dehumidification. The intention behind applying liquid desiccants (LD) is to avoid high latent loads on electrically driven compression chillers. For humid areas or under special needs of low humidity ratios, the condensation by subcooling and a downstream air reheating process can be avoided. The energy demand can be shifted to low grade heat as from solar or waste heat sources. The regeneration of these LD solutions is generally done in an open process; the desiccant is heated up and dried with ambient air, which results in poor regeneration efficiencies. Since MD has shown good performance for treatment of NaCl solutions near the saturation limit [1,2], the aim of this paper is to experimentally investigate its applicability in LDAC.

Starting with direct contact membrane distillation (DCMD) in the 1960s [3], a variety of different process configurations has been investigated during the last decades. The common component is a hydrophobic microporous membrane that separates a salty feed stream from a distillate or vapor channel. In DCMD, a temperature difference between feed stream and distillate stream is used to create a vapor pressure difference over the membrane. This leads to an evaporation of volatile components on the hot side of the membrane pores and their condensation on the cold side liquid surface. During this process, due to the hydrophobicity of the membrane material, no liquid should enter the membrane pores. [4,5]

Alternatively to DCMD, the vapor pressure gradient over the membrane can be created for example by a dry sweep gas or a reduction of the absolute pressure on the permeate side. Latter approach is called vacuum membrane distillation (VMD). [6] The removed vapor has to be condensed in a separate condenser, which can be used to determine the vacuum pressure level. If a cascade of VMD stages is connected in order to reuse the heat of condensation of one stage to heat up the feed for a next stage, the system resembles conventional multi-effect distillation (MED) and is called vacuum multi-effect membrane distillation (VMEMD). Summers and Lienhard [7] and Chung et al. [8] investigated the performance of a system similar to multistage flash (MSF) in a simulation study. The system contains external condensers and flash boxes. Their configuration allows a large number of stages due to the external condensers. This way, the simulation shows relatively high gained output ratios (GOR) and linear dependency of GOR on brine salinity. The investigations comprise brine salinities up to 26 m% NaCl.

In the present study, the investigated system by memsys [9] is using a triple channel setup that allows to build up a latent-sensible-latent heat and mass transfer configuration as known from MED plants. While steam of a previous stage condenses, it directly heats up the feed which evaporates over the membrane and produces steam at a lower pressure (compare Chapter 2). An extensive experimental study on the general behavior of the memsys module for treatment of seawater has been published by [10].

Generally, a gap of knowledge exists in literature concerning the applicability of VMD and especially VMEMD beyond vapor pressures reached with saturated solutions of NaCl. Several publications are available on experimental and numerical studies for bench scale VMD test cells [1,2,11,12], also concerning the effect of high salinity. Jang et al. [13] investigated the behaviour of a single stage VMD system with memsys' membrane block. Choo et al. [14] already used the memsys system for treatment of LiCl solutions up to 20 m% which is in terms of vapor pressure reduction comparable to a $CaCl_2$ solution at approximately 30 m%. Another approach towards application of MD in LDAC can be found in Rattner et al. [15]. They investigated the applicability of air gap membrane distillation (AGMD).

Since the solutions of $CaCl_2$ used in LDAC are generally in the vicinity of saturation, one major goal of this work is to determine the performance of the VMEMD system and to identify critical operating conditions in this region, also concerning crystallization fouling and membrane wetting. A wide-ranging variation of operation parameters is used to investigate their influence on the system performance, especially at feed concentrations between 30 and 45 m% $CaCl_2$. Additionally to a variation of the process boundary conditions, the number of stages has been varied. Latter has shown a significant influence on the performance and is one major parameter for system optimization concerning significant vapor pressure reduction. The experimental investigation is based on a theoretical analysis of the process in order to explain the physical behavior and to differentiate between physical phenomena and parasitic or system inherent side effects.

2. Multi-effect vacuum membrane distillation – working principle

As in all conventional membrane distillation configurations, the driving force is determined by the vapor pressure difference over the membrane, whereas the distillate side pressure in VMD approximately equals the partial vapor pressure, when a sufficient removal of non-condensable gases can be guaranteed [4,5]. The feed side equilibrium vapor pressure is depending on the solution temperature, salt concentration and salt species. It can be calculated from the saturation vapor pressure of pure water with help of the reduced water activity of the solution [16]:

$$p_{v,sol} = p_{sat}\left(w_s, T\right) = a\left(w_s, T\right) \cdot p_{sat,w}^{pure}\left(T\right) \tag{1}$$

It has to be kept in mind that generally used activity coefficient models such as Debye-Hückel and even Pitzer (as used with [17]) do not allow accurate calculation of activity coefficients for the range of $CaCl_2$ concentrations examined here. This is why, for further estimations, empiric correlations for all thermophysical properties collected and provided by [18] are used.

Furthermore, since for high concentrations the non-ideal solution behavior cannot be neglected anymore, the differential heat of mixing has to be included as a source term in the energy balance [19]. This differential enthalpy adds to the latent heat of vaporization and thus reduces the temperature in the feed channel.

2.1. System configuration

Similar to classical multi-effect distillation (MED), the vacuum multi-effect membrane distillation system (Fig. 1.) uses a sequence of effects at continuously lower operating pressure. This way, it is possible to use the latent heat of condensation of the steam produced in one effect to heat the feed water in the following effect. The vapor side pressure staging evolves due to the temperature differences between the effects. The distillate is collected in each effect and led to the next condenser channel over a throttle, where it partially flashes. The vapor from flashed distillate is reused in the condenser channel. This constructional detail only influences the performance in setups with three or more effects. In the two effect setup, the flashing of condensate from the second effect only leads to an additional load on the condenser.

The memsys system [9] uses a friction welded plate and frame setup consisting of three channel types in each effect (cf. Fig. 1.): The steam is condensed on a polypropylene foil in the condenser channel. Between this foil and a membrane, the feed channel is mechanically stabilized by a spacer. Finally, the third channel is on the vacuum side of the membrane, where the steam is led to the condenser channels of the next effect. The vacuum channel is mechanically stabilized by another grid, which also supports the membrane. This spacer has a significantly larger filament size in comparison to the feed spacer and brings room and stability for the vacuum channel. In order to scale up the membrane area, each effect might contain several of these channel combinations connected in parallel. A parallel connection of channels has the same effect as increasing the membrane width, when the feed flow velocity is kept constant. In contrast, an increase of the channel length would lead to a higher water recovery and therefore a change in temperature and concentration profiles over the channel length and finally to a different system behavior. Fig. 1. shows the functional principle with only one feed channel per effect. The original nomenclature by memsys is applied here. Streams are numbered with two digits, whereas the first digit denotes the stream and the second the position in the stream (e.g. before and after one effect). The heating circuit is stream number 1, so that the inlet to the steam raiser on liquid side is 11 and the outlet 12. In the same manner the feed is numbered with 2, brine with 3, distillate with 4, cooling water with 6 and the steam inside the effects with 7 (e.g. the steam produced by the first effect has the pressure p_{72}).

Experiments have been conducted on a setup with two and four effects. For simplicity, the balances of the two-effect system are discussed here. They can be easily extended to the four effect setup by adding the balances of the second effect for each following one. Fig. 2. shows a flow chart with all in- and outgoing streams for every effect. Thermal losses over the surface of the VMD block can be estimated to be below 5% of the steam raiser power in the range of investigated flow rates ($\dot{Q}_{V0} = 8$ kW, $T_{surf.,mean} \approx 40°C$, $\alpha_{surf.,mean} = 7$ Wm^{-2} K^{-1}, surface area of the VMD block with four effects $A_{surf.} = 2.56$ m^2). For very low feed flow rates the influence of these losses can increase significantly. The following balances can be used as an approximation, neglecting heat losses to ambient:

The steam raiser (SR) produces steam V0 that is used for heating of the feed in the first effect

$$\dot{Q}_{V0} = \dot{m}_{11} h_{11} - \left(\dot{m}_{11} - \dot{m}_{V0}\right) h_{12} \approx \dot{m}_{V0} h''_{sat}\left(p_{71}\right) \tag{2}$$

The steam is assumed to totally condense in the first effect without subcooling, while it preheats the feed 21 and

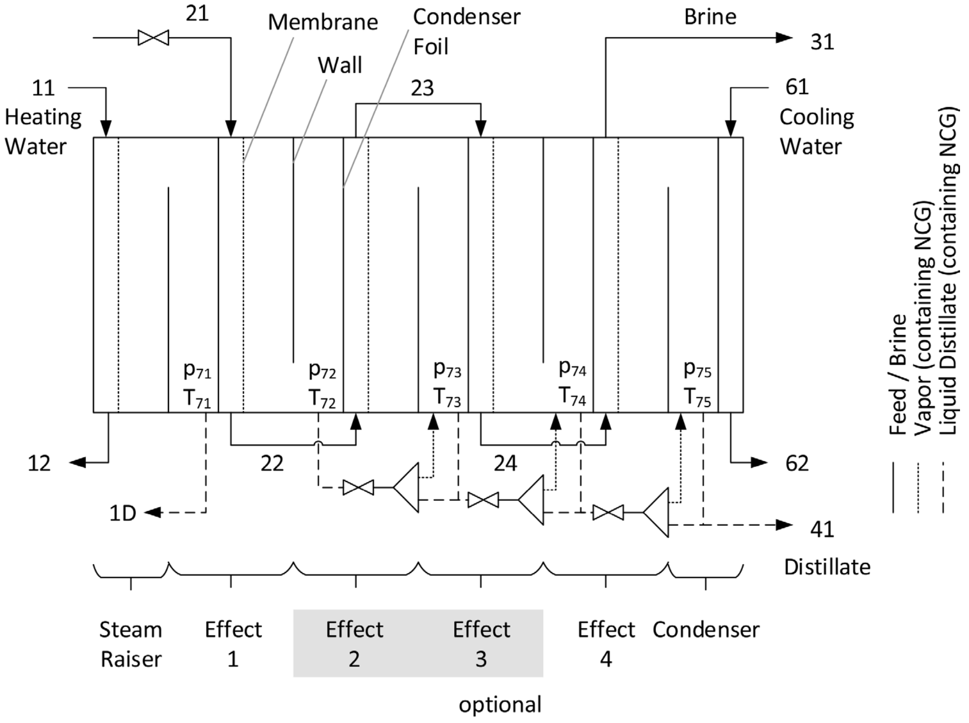

Fig. 1. Functional principle of the memsys VMEMD system as used for the experiments.

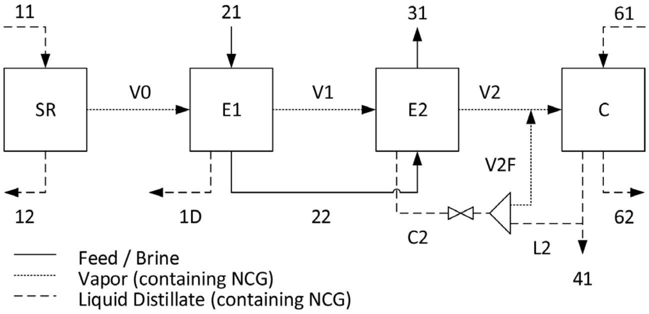

Fig. 2. Balances of the two-effect arrangement; streams named with indices.

afterwards constantly heats it while it partially evaporates over the membrane.

$$\begin{aligned}\dot{Q}_{cond,E1} &= \dot{m}_{V0}\,\Delta h_v\left(p_{71}\right) \\ &= \left(\dot{m}_{21}-\dot{m}_{V1}\right)h_{22}\left(T_{22},w_{22}\right) \\ &\quad+\dot{m}_{V1}\left(h''_{sat}\left(p_{72}\right)+\Delta h_{superheat,72}\right)-\dot{m}_{21}h_{21}\left(T_{21},w_{21}\right)\end{aligned} \tag{3}$$

The same balance can be written for the second effect neglecting subcooling of the condensate:

$$\begin{aligned}\dot{Q}_{cond,E2} &= \dot{m}_{V1}\,\left(\Delta h_v\left(p_{71}\right)+\Delta h_{superheat,72}\right) \\ &= \left(\dot{m}_{21}-\dot{m}_{V1}-\dot{m}_{V2}\right)h_{31}\left(T_{31},w_{31}\right)+\dot{m}_{V2}\,\left(h''_{sat}\left(p_{75}\right)\right. \\ &\quad\left.+\,\Delta h_{superheat,75}\right)-\left(\dot{m}_{21}-\dot{m}_{V1}\right)h_{22}\left(T_{22},w_{22}\right)\end{aligned} \tag{4}$$

If the condensate is assumed to be saturated liquid at the outlet of the condenser section of effect 2, the condenser is loaded with

$$\begin{aligned}\dot{Q}_{C} &= \dot{m}_{V2}\left(\Delta h_v\left(p_{75}\right)+\Delta h_{superheat,75}\right)+x_2\,\dot{m}_{V1}\,\Delta h_v\left(p_{75}\right) \\ &= \dot{m}_{61}\left(h_{62}-h_{61}\right)\end{aligned}, \tag{5}$$

if subcooling is neglected again and the throttling process is regarded isenthalpic. The flashing part of the condensate can be estimated with

$$x_2=\frac{h'\left(p_{72}\right)-h'\left(p_{75}\right)}{h''\left(p_{75}\right)-h'\left(p_{75}\right)}, \tag{6}$$

which adds to the vapor produced by effect 2 as

$$\dot{m}_{V2F}=x_2\,\dot{m}_{C2}\ . \tag{7}$$

The whole system, including the heating and cooling cycle, is operated at a pressure below ambient conditions in order to avoid large pressure differences over the condenser foils or membranes. The heat is mainly introduced into the system by the steam raiser which produces heating steam from distilled water over a membrane (as used in the effects). This steam is condensed in the first effect and heats up the feed water. The condensate is recirculated to the heating circuit. For the experimental setup the distilled water heating circuit is heated by an electrical heater, in order to simulate the heat input by solar or waste heat.

The steam that is produced in the last effect is condensed in the condenser. This condenser resembles the steam raiser, but with condenser foils instead of membranes. The adjacent heat rejection circuit is operated again with water and connected to a plate heat exchanger. This way, the whole system is isolated against ambient pressure. The feed enters over a valve and all outgoing streams are temporarily stored in tanks and pumped against ambient pressure.

In comparison to some experimental setups from literature, where the vacuum pump is used as driving force, here, the temperature difference between the steam raiser and the condenser defines the driving pressure difference. The vacuum pump is needed to remove the non-condensable gases, whereas the pressure in the steam channel of the last effect is defined by the condensation temperature level.

3. Influence of salt concentration on system behavior and optimization approach

In order to better understand the system behavior, the driving pressure and temperature differences can be plotted qualitatively according to Fig. 3. It shows the saturation vapor pressure curve of pure water and salt water (brine) with reduced vapor pressure. The gross driving pressure difference over each effect is the difference between the absolute pressures measured in the vapor chamber of the prior and the current effect ($\Delta p_{tot,i} = p_{v,i-1} - p_{v,i}$). For heat transfer over the foil, a temperature difference between the condensing steam and the bulk fluid in the feed channel ($\Delta T_{F,i} = T_{v,i-1} - T_{i,Brine}$) is necessary. Nevertheless, this value might significantly change over the length of a channel due to the latent-sensible configuration of the heat exchange. On the one hand, it is possible that the feed enters the effect at a temperature significantly below the condensation temperature, as it is the case for non-preheated feed (cp. section 6.1). On the other hand, when comparing to a setup that does not use continuous heating of the feed stream, the temperature drop over the channel length in each effect is reduced to a minimum, avoiding irreversibilities due to large temperature differences.

For a feed solution with negligible vapor pressure reduction, the driving pressure difference over the membrane can be calculated by $\Delta p_{Water,i} = p_{v,i,Water} - p_{v,i}$ which is the vapor pressure difference between that of pure water at the bulk feed temperature and that constituted by the condensation temperature level. The reduction of vapor pressure due to the salt content leads to a reduction of the driving pressure difference according to Eq. (1):

$$\Delta p_{Loss,i}=p_{sat}\left(T_{i,Brine}\right)-a\left(T_{i,Brine},w_{i,Brine}\right)p_{sat}\left(T_{i,Brine}\right) \tag{8}$$

This loss in driving pressure can also be written in terms of a temperature loss as $\Delta T_{Loss,i}$. The reduction of driving pressure difference due to reduced activity is inevitable and only depending on the temperature level and solute concentration and composition for a given system configuration. If a multi-effect configuration is used, this loss mechanism reduces the performance of each effect and sums up as follows:

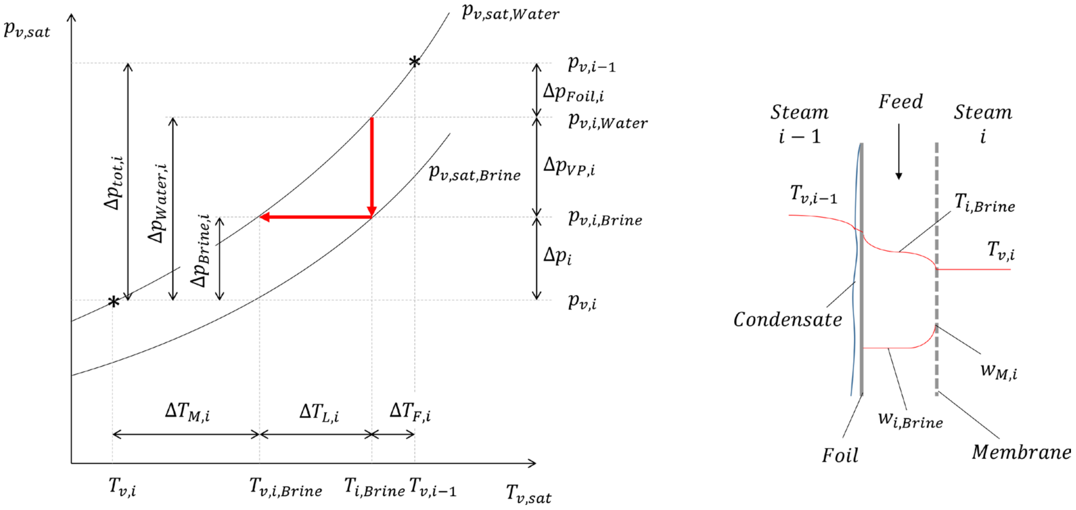

Fig. 3. Qualitative sketch of pressure and temperature differences over one effect (i) due to concentration dependent vapor pressure reduction, heat and mass exchange.

$$\Delta p_{Loss,tot} = \sum_{i=1}^{N_{effects}} \left(p_{v,sat}\left(T_{i,Brine}\right) - a\left(T_{i,Brine}, w_{i,Brine}\right) p_{v,sat}\left(T_{i,Brine}\right)\right) = \sum_{i=1}^{N_{effects}} p_{v,sat}\left(T_{i,Brine}\right)\left(1 - a\left(T_{i,Brine}, w_{i,Brine}\right)\right) \tag{9}$$

An averaging of the temperature and concentration over the length of an effect is only possible for low Recovery Ratios (RR)

$$\mathrm{RR} = \frac{\dot{m}_{distillate}}{\dot{m}_{feed}} = \frac{\dot{m}_{41}}{\dot{m}_{21}} \tag{10}$$

and low temperature differences.

In order to give a theoretical limiting salt concentration for a multi-effect setup under different operation conditions, the driving pressure can be assumed to be equally distributed between the effects. This is done mathematically by an iterative procedure. The resulting net driving pressure difference (NDPD) and net driving temperature difference (NDTD) for a one to six effect setup is shown in Fig. 4. It is calculated as

$$\mathrm{NDPD} = \sum_{i=1}^{N_{effects}} \left(p_i - p_{sat}\left(T_{sat}\left(p_i, 0m\%\right), w_i\right)\right). \tag{11}$$

An operation in multi-effect mode is only possible if heat transfer is guaranteed by a continuously falling temperature over the effects. This is not possible anymore for a larger number of effects at higher feed concentrations or low upper temperature levels. For the real plant operation these extreme boundary conditions will automatically set one or more effects out of order. The remaining absolute driving pressure and temperature difference can be used with the unfavorable effect of fallow membrane surface.

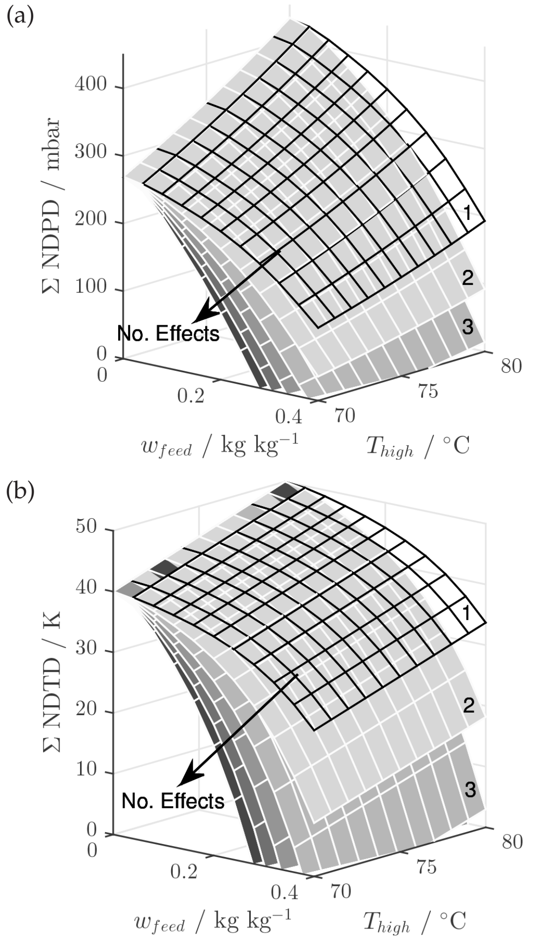

Fig. 4. Sum of NDPD and NDTD for setups with 2 to 6 effects at different upper temperature levels T_{high} (T_{low} = 30°C), feed concentrations w_{feed} for equally distributed pressure differences over the effects and RR → 0. (a) Sum of the net driving pressure differences (NDPD), (b) Sum of the net driving temperature differences (NDTD).

This theoretical assessment gives a hint on the decrease of plant performance due to vapor pressure reduction, since the sum of NDPD is directly proportional to the distillate production. Nevertheless, it has to be kept in mind that temperature polarization at the foil as well as concentration and temperature polarization at the membrane have to be overcome additionally.

Furthermore, a high number of effects can have a negative influence on the evaporation rate going along with reduced energy efficiency, when regarding the sensitivity on the temperature of heat rejection (here T_{low}). If a constant gross driving temperature difference (GDTD = $T_{high} - T_{low}$) is assumed and T_{low} is varied, for high concentrations an increase in T_{low} can have a negative influence on the NDPD and therefore on the distillate production as shown in Fig. 5. This effect is shifted to lower concentrations for the real process and can be observed in the analysis of measurement results in section 6.1. In the experiments, this effect is strongly increased by the necessity of feed preheating in the first effect, when the feed temperature is kept constant while rising the upper temperature level.

4. Experimental Setup

The experimental setup consists of a memsys R&D VMEMD test rig with a total membrane area (without steam raiser) of 6.4 m² in plate and frame configuration (Fig. 6.; for further information refer to [9]). It is equipped with sensors for temperature, pressure and conductivity measurement. Furthermore, each outgoing stream is led to a tank with a level control and a pump against ambient. This allows continuous operation under reduced pressures. The level control in the tanks is used for accurate time averaged flow measurement. The feed flow is adjusted with help of a rotameter, which allows direct contact with the highly corrosive fluids, but is strongly influenced by density and viscosity changes. Therefore, the real feed flow rate is calculated from the brine and distillate. The properties of the built-in GE Aspire microfiltration membrane can be found in Table 1.

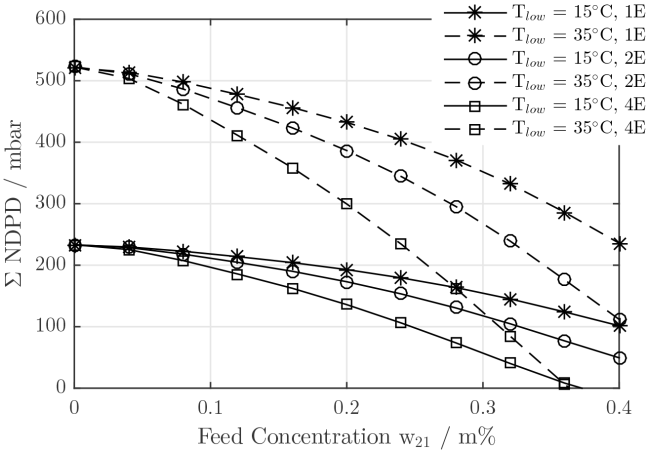

Fig. 5. Sum of net driving pressure differences (ΣNDPD) for a constant Gross Driving Temperature Difference GDTD = 50 K for 1, 2 and 4 effects and RR → 0.

The periphery and integration of the VMD block is shown in Fig. 6. Furthermore, all sensors referenced subsequently are shown here. For measuring brine and distillate flow rate, a mass balance of the brine (H) and distillate (I) vessels is used and automatically calculated with the trigger signal of the level sensors. This way, even for small mass flow rates and changing temperatures or salinities, accurate integral results can be reached.

The steam raiser is directly heated by a 17 kW [9] electric heater in order to simulate the low grade heat input. The actual steam raiser power is calculated as shown in Eq. (2) based on temperature and volume flow measurement. In order to reach a constant feed temperature even in batch operation, a plastic foil heat exchanger manufactured by memsys with an external heating circuit (sensible heating) is used to control the feed temperature. The heat rejection and thus the cold side temperature of the process can be controlled automatically by an additional valve which reduces the cooling water flow rate.

Experiments are conducted with a 2-stage as well as a 4-stage setup. Due to the constructional principle only an even number of effects can be realized. The concentration of the investigated salt solution is measured with inline conductivity meters for process surveillance. Due to a maximum value in the concentration dependency of the conductivity for aqueous solutions of $CaCl_2$ and high temperature dependency, no accurate concentration determination is possible with this technique. Therefore, probes are taken and evaluated with a Mettler-Toledo (RE40) benchtop refractometer. Here, a linear dependency of refraction index on salt concentration leads to accurate results.

5. Experimental Procedure

Steady state measurements are chosen for performance evaluation in order to use the above described level sensor based flow rate measurement. Batch experiments are conducted at constant feed concentration. When a stationary temperature in each effect is reached (after approx. 15–30 min), a measurement period of 30–60 min is averaged. Transient behavior is investigated by step responses and temperature measurement.

A matrix with experiments under variation of the following variables has been designed: Heating circuit inlet temperature, feed temperature, feed mass flow rate, feed concentration and condenser circuit inlet temperature. As constructional boundary condition, only the number of effects is varied between two and four.

6. Results

In the following, the results of the steady state measurements are evaluated. With regard to an optimization for application in desiccant regeneration or zero liquid discharge, high performance ratios, operational safety as well as cost effectiveness have to be regarded. Therefore, experiments at lower concentrations are conducted, too. The effective determination of an optimal operation concentration in a liquid desiccant air conditioning plant hast to be discussed from an economic point of view elsewhere.

Performance can be measured with the gained output ratio (GOR, Eq. (12)), specific energy consumption (SEC,

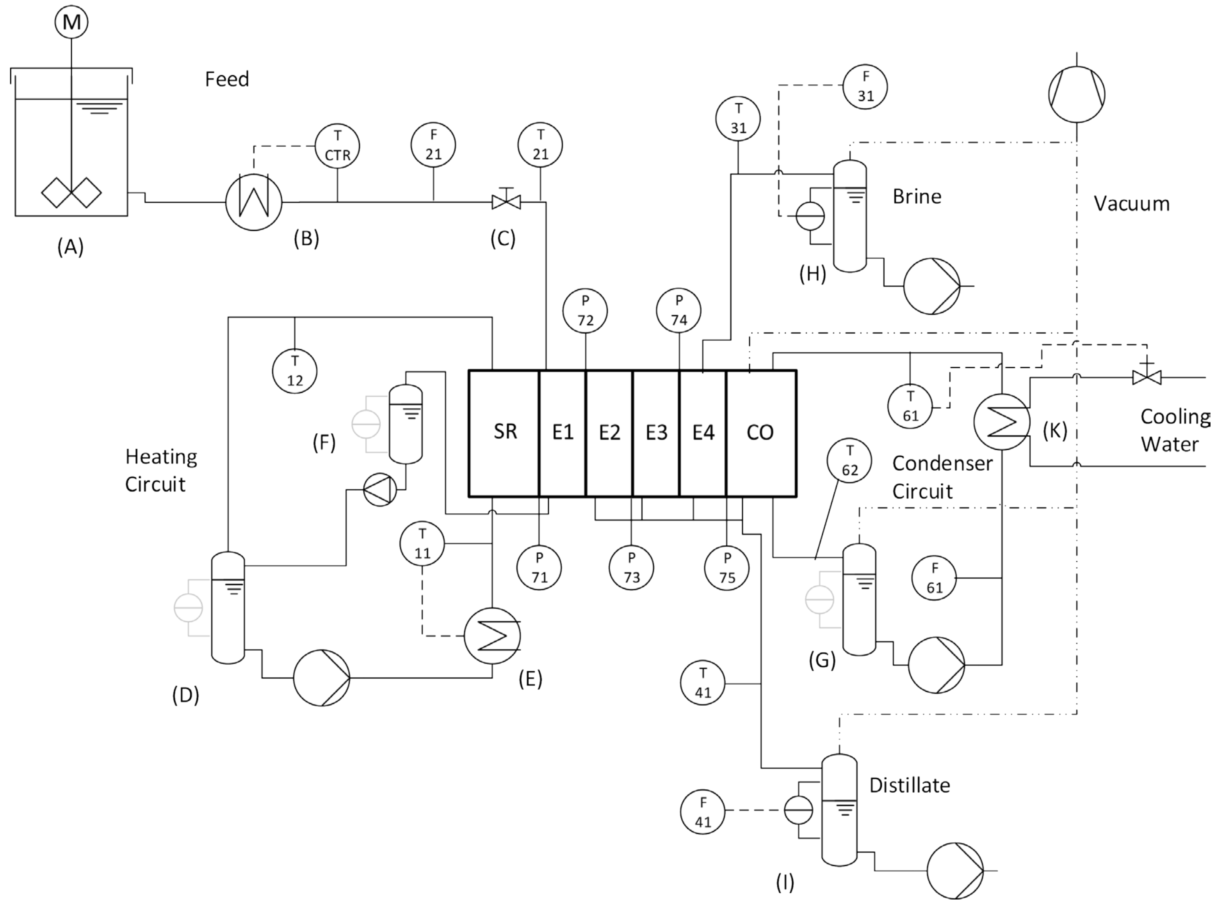

Fig. 6. Piping and instrumentation diagram of the experimental setup containing additional feed and cooling temperature control. SR: Steam Raiser, E1–E4: Effects, CO: Condenser. (A) feed tank, (B) feed preheating with temperature control, (C) inlet throttle valve, (D) heating circuit compensation reservoir, (E) electrical heater with temperature control, (F) heating steam distillate recovery, (G) condenser circuit compensation reservoir, (H) brine tank with level control and flow calculation, (I) distillate tank with level control and flow calculation. (Adapted from [9]).

Eq. (13)) and Recovery Ratio (RR, Eq. (10)) as usual in desalination systems. For GOR the commonly used reference enthalpy $\Delta h_{v,0}$ = 2326 kJ/kg has been chosen. For the SEC the preheating from ambient temperature (T_{∞} = 25°C) to the constant feed temperature (T_{21} = 50°C) is taken into account as $\dot{Q}_{preh}$.

$$\mathrm{GOR} = \frac{\dot{m}_{41}\,\Delta h_{v,0}}{\dot{Q}_{V0}} \tag{12}$$

Table 1
Membrane specifications according to [20]

Hydrophobic ePTFE Membrane Laminate	Product Type QL822
Vendor	GE Energy
Active layer	PTFE
Backing material	PP
Reference pore size	0.2 µm
Thickness	0.12–0.22 mm
Water entry pressure	> 3.5 bar

$$\mathrm{SEC} = \frac{\dot{Q}_{V0} + \dot{Q}_{preh.}}{\dot{m}_{21}} \tag{13}$$

6.1. Influence of operation parameters

Firstly, the feed inlet and heat rejection temperature are held constant, (T_{21} = 50°C, T_{61} = 30°C). In order to allow comparison of different measurements, the energy for feed preheating from ambient temperature (T_{∞} = 25°C) to T_{21} is included in the SEC. As a reference for salt experiments, measurements with distilled water are shown in Fig. 7. in the first column. Steady-state measurements for the 2-effect setup (Fig. 7. first row) and 4-effect setup (Fig. 7. second row) are taken.

It can be observed, that at constant boundary conditions the highest distillate output can be generated for a feed concentration of 0 m% $CaCl_2$ with the 4-effect setup. Nevertheless, this changes for high salt concentrations (Fig. 7. second column). At 30 m% the 4-effect plant still produces a reliably measurable amount of distillate, but clearly under-performs the 2-effect setup. A second observation can be made concerning the feed flow rate. Whereas for low feed concen-

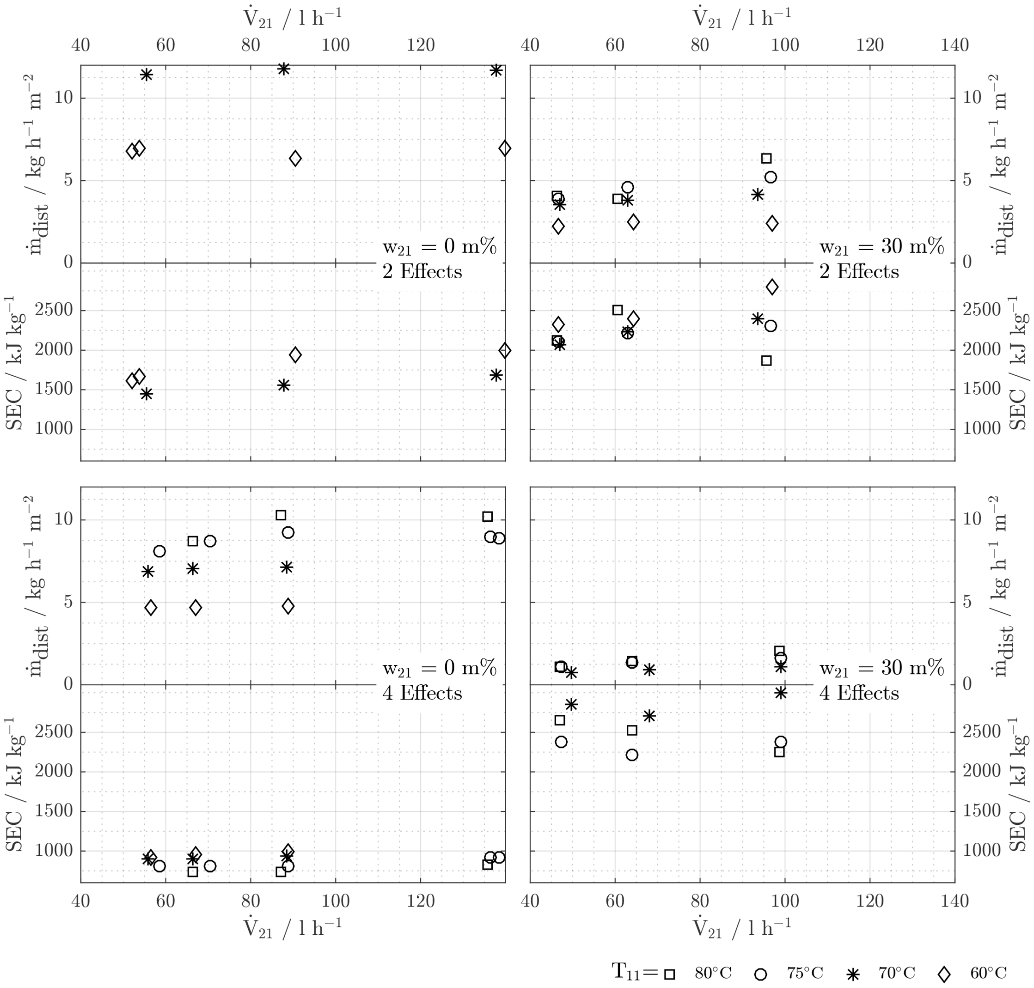

Fig. 7. Dependency of the distillate production $\dot{m}_{dist}$ and specific energy consumption SEC on feed flow rate $\dot{v}_{21}$. SEC includes preheating from 25°C to 50°C. Left column: 0 m% $CaCl_2$ feed concentration; right column: 30 m% $CaCl_2$ feed concentration; first row: 2-effect setup; second row: 4-effect setup.

trations a theoretical RR of 100% is possible, it is strongly limited for higher feed concentrations. For the 2-effect configuration nearly no influence of the feed flow rate on the distillate output can be measured; the 4-effect setup already shows an influence at higher heating temperatures. This can be explained by a reduction of the effective feed temperature in the first effect.

The SEC generally rises with rising feed flow rate mainly due to lower recovery ratio and thus larger enthalpy of brine stream. For higher concentrations using a four-stage setup, this effect can be counterbalanced by the significant reduction of the driving pressure difference over each stage and the accompanying effects. For high concentrations additionally the concentration polarization and the continuously rising concentration of the salt solution throughout the plant lead to a decrease in distillate output. Now, higher feed flow rates lead to a lower RR and thus lower Concentration Factor (CF) over the module.

Generally, the influence of feed flow rate rises significantly with rising difference between feed temperature and heating circuit temperature due to necessary preheating and reduction of the pressure of the first effect as well as with rising distillate production. In the first effect the amount of heat in terms of produced steam that can be reused in the subsequent stages can be measured. At the same time the power of the steam raiser is influenced by the feed inlet temperature and mass flow rate in combination with the amount of steam produced in the first effect.

In order to compare the influence of the steam raiser temperature level and the temperature level of heat rejection on the process performance, for the four effect setup at 35 m% $CaCl_2$ the condenser inlet temperature T_{61} is varied while keeping a constant gross driving temperature difference GDTD = $T_{11} - T_{61}$. The results are shown in Fig. 8. A reduction of the cooling water temperature level results in a higher performance enhancement than could be achieved by rising the heating temperature level as already predicted for the multi-effect setup at high concentrations in Fig. 5. Additionally, since the feed temperature is kept constant, with rising temperature level of the steam raiser, more power is needed for feed preheating in the first effect. This significantly adds to the aforementioned effect.

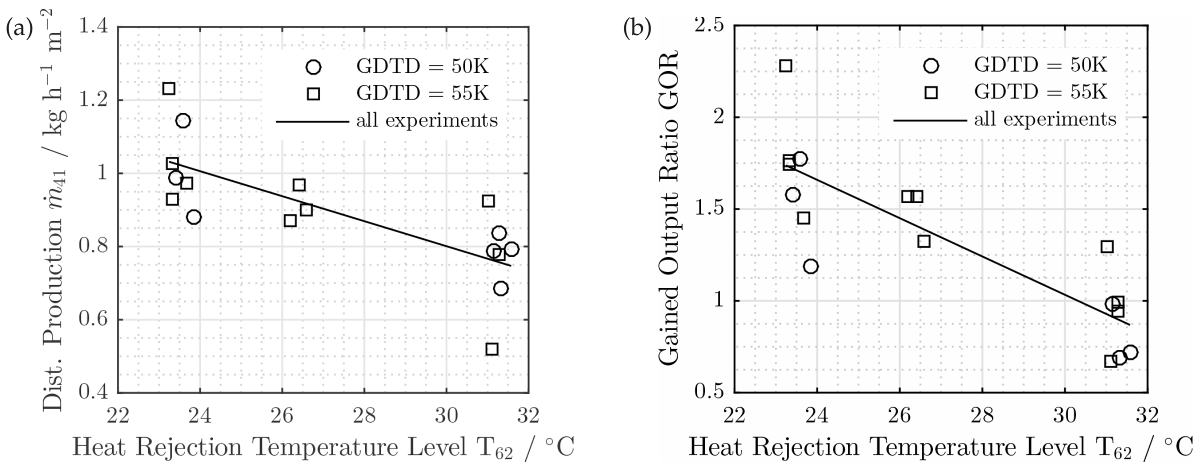

Fig. 8. Sensitivity on heat rejection temperature level for constant gross driving temperature differences GDTD = $T_{11} - T_{61}$ with the 4-effect setup at a feed concentration of 35 m%. (a) Distillate production $\dot{m}_{41}$, (b) Gained output ratio.

6.2. Concentration dependency

A comparison of the vapor pressures from steady-state measurements at 60°C for the complete span of feed concentrations is shown in Fig. 9. For the two-effect setup p_{72}, is the pressure of the vapor produced in effect 1, effects 2 and 3 are taken out of the machine and therefore p_{75} is the steam pressure of effect 2. Pressures with index *sat* are calculated from temperature and concentration measurement. The experiments at 60°C are well suited for this analysis, since the influence of the feed flow rate of a subcooled feed is minimized. The following observations can be made:

- The steam pressure p_{71} produced by the steam raiser is constantly rising with rising feed concentration. Since the mass flow rate in the steam raiser stays constant, this is caused by a decrease in evaporation power in the first effect.
- The constant value $p^{\text{pure}}_{(\text{sat},21)}$ of is the vapor pressure of pure water at the temperature of the feed solution, which is controlled to 50°C. It can be observed, that for low concentrations the effect of feed preheating is not as big as for higher values.
- For high concentrations the feed enters the plant with an equilibrium vapor pressure significantly below the pressure level of the first effect.
- The first effect (including heat transfer from the steam raiser) has the biggest influence on absolute driving pressure reduction.
- The highest cooling water temperature determines the pressure level of condensation.

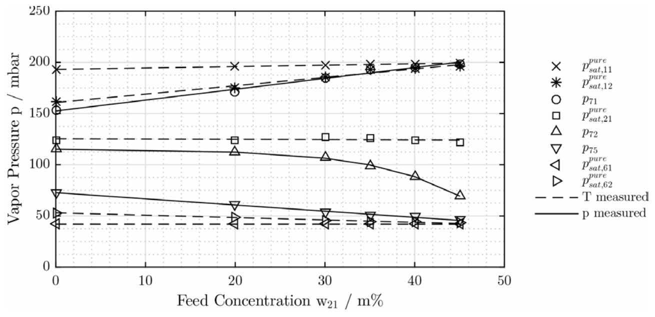

Fig. 9. Concentration dependency of measured vapor pressures in the two-effect setup.

The performance dependency on top temperature level (steam raiser inlet temperature) is shown in Fig. 10. As already observed in Fig. 7. the influence of the feed flow rate on the distillate production has a minor effect for low feed concentrations. With rising top temperature level, the distillate production rises due to higher driving pressure difference. This increase is significantly reduced for higher concentrations due to the nonlinear reduction of the equilibrium vapor pressure of the feed and the multiplication of boiling point elevation associated performance reduction by the number of effects (here with a factor of 2).

Furthermore, Fig. 10. shows the possible field of operation of the plant with two effects. For distilled water, the highest temperature was limited to 70°C by the maximum heating power of the electrical heater. GOR is increased with rising upper temperature level (at constant condenser temperature) and therefore greater driving pressure difference for low and medium concentrations. For very high concentrations a drop in GOR can be observed. The explanation therefore is again the larger influence of absolute vapor pressure reduction at higher temperatures and its multiplication for multiple effects. Additionally, since the feed temperature is held constant, the feed preheating inside the first effect is more dominant for higher upper temperature levels and thus reduces the GOR.

The reduction of distillate production with rising feed concentration can be observed in Fig. 11. For higher feed concentrations the distillate production of the 4-effect setup is significantly lower than that of the 2-effect system. This will be discussed in detail in the next section.

6.3. Influence of number of effects

When comparing Fig. 11. with the theoretical analysis of the reduction of the net driving vapor pressure difference over a multi-effect system in Fig. 4. it becomes obvious that

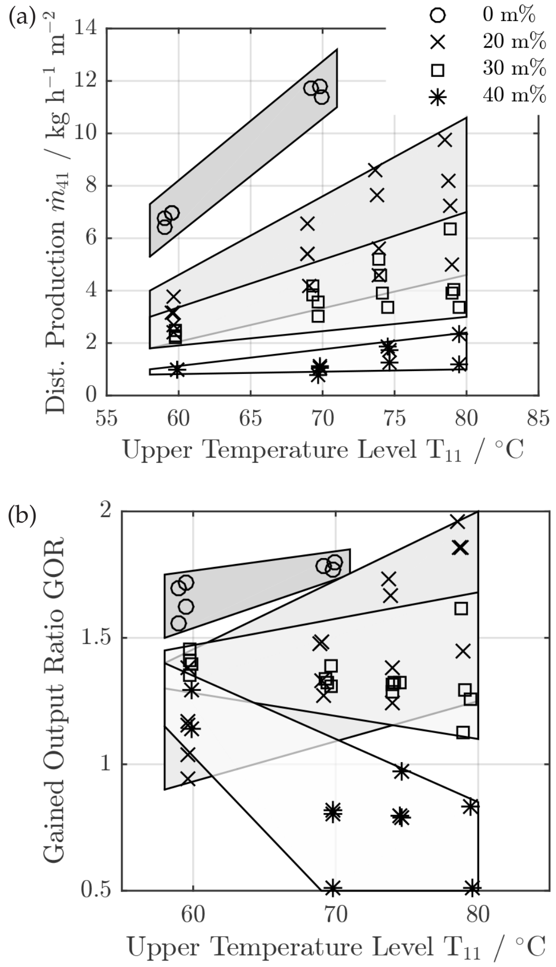

Fig. 10. Overview and limits of operation for the 2-effect setup at different feed flow rates. (a) Dependency of distillate production on heating temperature and feed concentration, (b) Dependency of Gained Output Ratio on heating temperature and feed concentration.

the experiments do not correlate with the shape of the theoretically estimated decline in distillate production. For high feed concentrations, theory shows a steeper slope at higher concentrations. This discrepancy can only be explained by a quasi-reduction of the effective number of stages in the system where heat and mass transfer takes place. This self-regulating mechanism should be investigated in detail elsewhere.

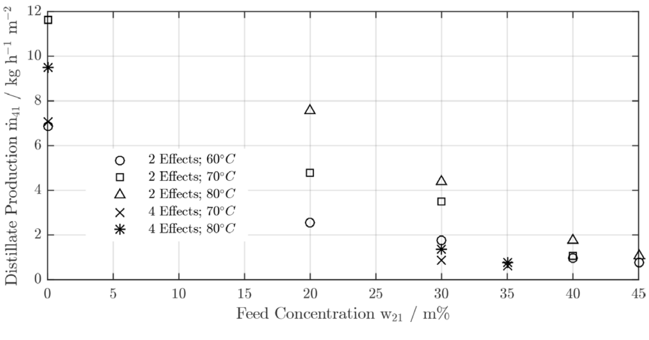

Fig. 11. Specific distillate production per square meter membrane area for steady state experiments at different $CaCl_2$ concentrations (averaged over feed flow rate). Experiments with distilled water (0 m% salt concentration) are limited to lower temperatures due to high steam raiser power.

6.4. Operation limits

During more than twelve months of operation up to feed concentrations of 40 m% $CaCl_2$ no leakages by wetting (entrance of feed solution into the membrane) or membrane destruction could be detected. Therefore, probes of distillate directly in the evaporation channel have been measured after disassembling the effects. Nevertheless, for higher concentrations the cool-down of the plant is not possible anymore without crystallization. This is why for the 45 m% experiments the plant has been rinsed before shutdown. Possible spots for crystallization of the primary electrolyte (here $CaCl_2$) are the cold feed inlet of effect one, regions with high flux, as occurring at the inlet of each following effect and at the outlet of the system with the highest brine concentration. Since the VMD block is opaque, intermediate positions could not be observed for crystal growth. At the feed inlet and brine outlet no crystallization was observed for operational conditions as stated before.

Generally, the operation limit is determined by heating and heat rejection temperature. When comparing the solubility boundary with possible heat rejection temperatures and the equilibrium vapor pressures of $CaCl_2$ at these temperatures, very low condenser temperatures are necessary to reach crystallization limit in continuous operation. Thus, for application in LDAC safe operation for aqueous $CaCl_2$ and LiCl even at high concentrations is possible. This will not apply for NaCl, where saturation limit will be easily reached.

The channel construction limits the maximum feed flow rate, since non-predictable behavior of the channel for high flow rates due to missing mechanical stabilization occurs. A detachment of spacer, foil and membrane is assumed to take place when the pressure drop in the feed channel leads to higher absolute pressures than the pressure difference established between two adjacent effects. This does not happen for moderate flow rates, since the spacer compression is held up by the pressure difference over the effect.

Due to the plant specific setup, the saturation temperature at vacuum pressure of the first effect should not be reached before entering the effect. Otherwise the feed already flashes at the inlet throttle valve. The upper temperature limit is determined by the water heating circuit as well as the construction material (PP). The maximum value for T_{11} is set to 80°C. At low feed concentrations the plant specific maximum temperature is further limited by the power of the electrical heater.

The lower temperature limit is determined by the cooling water temperature and mass flow rate. In order to simulate the application area (cooling with seawater or air chiller), a relatively high temperature level of has been chosen. The temperature difference over the plate heat exchanger has to be subtracted to get the external temperature level of heat rejection.

6.5. Generalization on vapor pressure dependency

The findings can be transferred to a dependency on saturation vapor pressure of any feed solution when translating salt concentrations to equilibrium vapor pressures and neglecting parasitic effects like heat of mixing that differs between different electrolytes. According to [18], the differential enthalpy of dilution, which adds to the heat of vaporization of pure water, significantly rises towards the crystallization boundary for solutions of LiCl and $CaCl_2$. At 40 m% it reaches at 20°C (75°C) approx. 117.3 $\text{kJ kg}^{-1}_{H_2O}$ (190.7 $\text{kJ kg}^{-1}_{H_2O}$) for $CaCl_2$ and 256.8 $\text{kJ kg}^{-1}_{H_2O}$ (283.4 $\text{kJ kg}^{-1}_{H_2O}$) for LiCl. For aqueous NaCl at 25°C it has a maximum near 25 m% of approx. 5.1 $\text{kJ kg}^{-1}_{H_2O}$ [21] and is therefore negligible.

Fig. 12. shows the equilibrium vapor pressure above aqueous solutions of NaCl, $CaCl_2$ and LiCl at two different temperatures. Three characteristics should be carved out here: The slope of NaCl and $CaCl_2$ is almost equal up to the saturation limit of NaCl. The effective vapor pressure reduction is relatively low for solutions of NaCl with a safety margin to onset of crystallization. For dehumidification purposes $CaCl_2$ is therefore preferred due to its high solubility. Solutions of LiCl show a much steeper slope of the vapor pressure curve over concentration. With a concentration of approximately 30 m% the same vapor pressure reduction can be reached as with $CaCl_2$ at 40 m%.

Finally, the absolute vapor pressure reduction at a temperature determines the above described exponential reduction of the sum of net driving pressure differences over the module. It is dominating at high salt concentrations and high temperatures.

7. Summary and concluding remarks

The experimental and theoretical analysis of the VMEMD system shows the benefits of a multi-effect configuration at low and medium feed concentrations. For application in regeneration of liquid desiccants, such as calcium or lithium chloride solutions where the multiplication of irreversibilities induced by vapor pressure reduction is the prevailing loss mechanism, a careful design is necessary. With rising feed concentration, the number of effects has to be reduced in order to reduce losses which are overwhelming the advantages of a multi-effect setup.

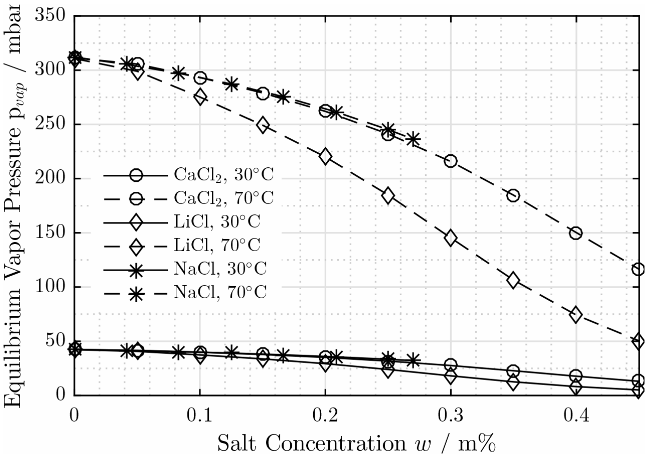

Fig. 12. Equilibrium vapor pressure over aqueous solutions of NaCl (calculated according to [17]) up to a solubility limit of approx. 28 m% at average operating temperatures, $CaCl_2$ and LiCl (calculated according to [18]) at 30 and 70°C.

Due to the high solubility of $CaCl_2$ at the investigated temperatures, a safe operation without membrane wetting is possible. Since the plant is constructed of polypropylene or PTFE in all parts in contact with the desiccant solution, the high corrosiveness does not present a restriction. Besides the adjustment of the number of effects, a reduction of the temperature level of heat rejection and a preheating of the feed solution should be focused on.

For application in LDAC the use of intermediate concentrations of $CaCl_2$ or LiCl is suggested. For application in ZLD with NaCl as primary electrolyte, the shown effects of ultra-high concentrations reached with $CaCl_2$ will not be predominant for setups with four effects or less. Therefore, the operation range will be strongly limited by a necessary safety margin to the onset of crystallization fouling. For $CaCl_2$ this is only possible with a reduced number of effects and due to a strongly temperature dependent solubility boundary. Because of extremely low saturation vapor pressures of LiCl, it is not expected to be possible to reach the solubility limits with reasonable condenser temperatures.

For optimization of the operating conditions a reduction of the condenser temperature should be preferred to increasing the heating temperature. The main influencing factor concerning the upper temperature level at high concentrations is the feed temperature in combination with the feed flow rate. Especially for high feed flow rates, a feed preheating is strongly recommended. The preheating temperature level should be near the vapor temperature of the first effect and has to be adjusted iteratively, to reach an optimum.

Acknowledgments

The authors gratefully acknowledge financial support from the German Federal Ministry of Education and Research (BMBF) in the project TUNGER-SPACE (FKZ O1DH13019) within which this paper was developed. The responsibility for the content stays with the authors. Special thanks go to memsys GmbH for providing the test plant and continuous technical support.

Symbols

Abbreviations

GOR — Gained output ratio
LD — Liquid desiccant
LDAC — Liquid desiccant air conditioning
NCG — Non-condensable gases
NDPD — Net driving pressure difference
NDTD — Net driving temperature difference
RO — Reverse osmosis
RR — Recovery ratio
SEC — Specific energy consumption
SR — Steam raiser
VMD — Vacuum membrane distillation
VMEMD — Vacuum multi-effect membrane distillation
ZLD — Zero liquid discharge

Variables

a	—	Solvent activity
A	—	Area
α	—	Heat transfer coefficient
h'	—	Specific enthalpy saturated liquid
h''	—	Specific enthalpy saturated vapor
$\dot{m}$	—	Mass flow rate
p	—	Pressure
$\dot{Q}$	—	Heat flow rate
T	—	Temperature
$\dot{V}$	—	Volume flow rate
w	—	Mass fraction
x	—	Steam quality

Indices

11, 12	—	Steam raiser cycle in-, outlet
21	—	Feed inlet
31	—	Brine outlet
41	—	Distillate outlet
61, 62	—	Cooling cycle in-, outlet
71	—	Steam produced by SR
72-75	—	Steam produced by effect 1–4
dist	—	Distillate
preh	—	Preheating
sat	—	Saturation
sol	—	Solution
surf.,mean	—	Mean property at VMD block surface
v	—	Vapor
∞	—	Ambient conditions

References

[1] M. Safavi, T. Mohammadi, High-salinity water desalination using VMD, Chem. Eng. J., 149 (2009) 191–195.

[2] J.-P. Mericq, S. Laorie, C. Cabassud, Vacuum membrane distillation of seawater reverse osmosis brines, Water Res., 44 (2010) 5260–5273.

[3] M. Findley, Vaporization through porous membranes, I&EC Process Design Develop., 6(2) (1967) 226–230.

[4] M.S. Khayet, T. Matsuura, Membrane Distillation: Principles and Applications, Elsevier, Amsterdam, 2011.

[5] K. Nikolaus, Trink- und Reinstwassergewinnung mittels Membrandestillation, Volume 10 of Fortschritt-Berichte, Techn. Univ. Kaiserslautern, 2013.

[6] K.W. Lawson, D.R. Lloyd, Review membrane distillation, J. Membr. Sci., 124 (1997) 1–25.

[7] E.K. Summers, J.H. Lienhard, Cycle Performance of multi-stage vacuum membrane distillation (MS-VMD) systems, The International Desalination Association World Congress on Desalination and Water Reuse, Tianjin, China, 2013.

[8] H.W. Chung, J. Swaminathan, D.M. Warsinger, J.H. Lienhard, Multistage vacuum vembrane distillation (MSVMD) systems for high salinity applications, J. Membr. Sci., 497 (2016) 128–141.

[9] Memsys clearwater Pte. Ltd., "memDist 4-6.4 - Technical description of process, modules and applications," 2015. Available under: http://www.memsys.eu/dateien/products/memsys_datasheet_4_6_4.pdf. [Accessed 03.06.2015].

[10] K. Zhao, W. Heinzl, M. Wenzel, S. Büttner, F. Bollen, G. Lange, S. Heinzl, N. Sarda, Experimental study of the memsys vacuum-multi-effect-membrane-distillation (V-MEMD) module, Desalination, 323 (2013) 150–160.

[11] J.I. Mengual, M. Khayet, M. Godino, Heat and mass transfer in vacuum membrane distillation, Int. J. Heat Mass Trans., 47 (2004) 865–875.

[12] J.-P. Mericq, S. Laorie, C. Cabassud, Vacuum membrane distillation for an integrated seawater desalination process, Desal. Water Treat., 9 (2009) 287–296.

[13] E. Jang, S.-H. Nam, T.-M. Hwang, S. Lee, Y. Choi, Effect of operating parameters on temperature and concentration polarization in vacuum membrane distillation process, Desal. Water Treat., 54 (2015) 871–880.

[14] F.H. Choo, M. KumJa, K. Zhao, A. Chakraborty, E.T.M. Dass, M. Prabu, B. Li, S. Dubey, Experimental study on the performance of membrane based multi- effect dehumidifier regenerator powered by solar energy, Energy Procedia, 48 (2014) 535–542.

[15] A.S. Rattner, A.K. Nagavarapu, S. Garimella, T.F. Fuller, Modeling of a flat plate membrane-distillation system for liquid desiccant regeneration in air-conditioning applications, Int. J. Heat Mass Transfer, 54 (2011) 3650–3660.

[16] P.W. Atkins, Atkins' Physical Chemistry, 10th ed., Oxford University Press, Oxford, 2014.

[17] D.L. Parkhurst, C.A.J. Appelo, Description of Input and Examples for PHREEQC Version 3 - A Computer Program for Speciation, Batch-Reaction, One-Dimensional Transport and Inverse Geochemical Calculations, in U.S. Geological Survey Techniques and Methods, U.S. Department of the Interior, U.S. Geological Survey, Denver, Colorado 2013, book 6, chap. A43.

[18] M.R. Conde, Aqueous solutions of lithium and calcium chlorides: property formulations for use in air conditioning equipment design, Int. J. Thermal Sci., 43 (2004) 367–382.

[19] W. Kessling, Luftentfeuchtung und Energiespeicherung mit Salzlösungen in offenen Systemen, Fortschritt-Berichte VDI, 3 ed., vol. 509, Verfahrenstechnik VDI, Düsseldorf, 2009.

[20] General Electric Company, Aspire (TM) Microfiltration Membranes - data sheet, Product QL833, 2007.

[21] P. Stephan, K. Schaber, K. Stephan, F. Mayinger, Thermodynamik, Grundlagen und technische Anwendungen, Band 2: Mehrstoffsysteme und chemische Reaktionen, Springer, Heidelberg, 2010.

[22] M. Khayet, T. Matsuura, Pervaporation and vacuum membrane distillation process: modeling and experiments, AIChE J., 50(8) (2004) 1697–1712.

[23] K. Lawson, D. Lloyd, Membrane distillation. I. Module design and performance evaluation using vacuum membrane distillation, J. Membr. Sci., 120 (1996) 111–121.